Corrosion Science 134 (2018) 131–139

Contents lists available at ScienceDirect

Corrosion Science

journal homepage: www.elsevier.com/locate/corsci

Short Communication

Corrosion behavior of an equiatomic CoCrFeMnNi high-entropy alloy compared with 304 stainless steel in sulfuric acid solution

Hong Luo*, Zhiming Li*, Andrea M. Mingers, Dierk Raabe

Max-Planck Institut für Eisenforschung, Max-Planck Str. 1, D-40237 Düsseldorf, Germany

ARTICLE INFO

Keywords:
A. Alloy
B. XPS
C. Corrosion
C. Acid corrosion

ABSTRACT

The corrosion resistance and passive film properties of an equiatomic CoCrFeMnNi high-entropy alloy (HEA) compared with 304L stainless steel in 0.1 M H_2SO_4 solution were investigated. The in-situ element-resolved corrosion analysis shows that selective dissolution of elements in the HEA is not evident compared to a 304 L stainless steel during passivation. The passive film formed on the HEA is enriched in Fe and Mn but depleted in Cr. The low content of Cr and the extensive formation of metal hydroxide in the passive film are responsible for the lower anti-corrosion performance of the HEA.

1. Introduction

High-entropy alloys (HEAs) were originally designed as alloys composed of multiple principal elements in equimolar or near-equimolar ratios where the high mixing entropy serves in stabilizing them in disordered massive solid solution state [1,2]. Over the past decade, this concept has attracted considerable attention as it provides enormous compositional opportunities for designing novel materials with beneficial mechanical properties [3–5]. Accordingly, various HEAs have been developed during the past years, e.g., face-centered cubic (FCC) CoCrFeMnNi [6] and body-centered cubic (BCC) VNbMoTaW [7] alloy systems. Among these, the FCC structured equiatomic CoCrFeMnNi HEA which was first reported by Cantor et al. [2], has particularly excellent mechanical properties at cryogenic and room temperature [4].

Recently, the corrosion behavior of some types of HEAs in aqueous solution has been reported. Shih et al. [8] revealed that the corrosion resistance of $Al_xCrFe_{1.5}MnNi_{0.5}$ (x = 0, 0.3, 0.5 at.%) HEAs in H_2SO_4 and NaCl solutions enhances as the concentration of aluminium decreases from 0 to 0.5 at.%. The pitting corrosion behavior of a $Co_{1.5}CrFeNi_{1.5}Ti_{0.5}Mo_{0.1}$ HEA in chloride-containing sulphate solutions studied by Yeh et al. shows that the values of the pitting potential change in a linear manner with the logarithm of the chloride concentration at 70 °C and 80 °C [9]. Moreover, the influence of the Al content on stable/metastable pitting of an $Al_xCoCrFeNi$ (x = 0.3, 0.5, 0.7 at.%) HEA in a 3.5 wt.% NaCl solution was investigated by Liwa [10]. Also, Grewal, et al. [11] demonstrated the cavitation erosion-corrosion behavior of the $Al_{0.1}CoCrFeNi$ HEA in 3.5 wt.% NaCl. Very recently, Rodriguez et al. [12] investigated the corrosion behavior of the group of CoCrFeMnNi HEAs in acidic sodium chloride solution with CO_2. They showed that the Cr content plays an important role on the corrosion rate of the HEAs. In addition, the corrosion properties of the CoCrFeMnNi HEA coating in 3.5 wt.% NaCl solution has been evaluated [13] and it was shown that the element segregation exhibits harmful effects on the corrosion resistance of the HEA coating.

It is well known that the surface of binary Fe-Cr alloys can be rendered passive when the Cr content is above 12 at.% [14]. The excellent corrosion resistance of austenite stainless steels with a Cr content above 12 at.% is also due to the formation of a protective thin passive film on its surface when exposed to the corrosive environment [15]. The corrosion and electrochemical behavior of stainless steel in various environments have been well characterized [15–18]. Interestingly, the equiatomic CoCrFeMnNi HEA contains similar corrosion-resistant elements, i.e., Cr and Ni as the standard AISI 304 austenite stainless steel (72Fe-19Cr-9Ni). Also, they both have a single-phase FCC structure with similar lattice parameter (~0.36 nm [19]). Although very recently Rodriguez et al. [12] investigated the corrosion properties of the CoCrFeMnNi HEA family in acidic sodium chloride solution, detailed information such as the fundamental mechanisms associated with the composition and structure of the passive film are still unknown. Yet it is of interest to fundamentally understand the corrosion behavior of the equiatomic CoCrFeMnNi HEA in comparison with the well-established 304L SS considering their similar corrosion-resistant elements (Cr and Ni) and single FCC lattice structure.

Motivated by the above considerations, in this work we investigated the corrosion behavior of the equiatomic CoCrFeMnNi HEA compared with the 304 L stainless steel in 0.1 M H_2SO_4 solution by combining a micro-electrochemical scanning flow cell (SFC) and an inductively

* Corresponding authors.
E-mail addresses: h.luo@mpie.de (H. Luo), zhiming.li@mpie.de (Z. Li).

https://doi.org/10.1016/j.corsci.2018.02.031
Received 13 June 2017; Received in revised form 9 February 2018; Accepted 16 February 2018
Available online 21 February 2018
0010-938X/

Table 1
Compositions of HEA and 304L SS according to wet-chemical analysis (wt.%).

Elements	C	Cr	Ni	P	S	Co	Mn	Fe
HEA	–	18.6	20.9	–	–	21.1	19.5	19.9
304 L SS	0.006	18.15	8.04	0.015	0.005	–	0.35	73.43

coupled plasma mass spectroscopy (ICP-MS) element analysis. The passivation behavior and composition of the passive film of the equiatomic CoCrFeMnNi HEA were investigated by electrochemical impedance spectroscopy (EIS) and X-ray photoelectron spectroscopy (XPS), respectively. Our main aim is to identify the corrosion mechanism of the equiatomic CoCrFeMnNi HEA.

2. Experimental procedures

2.1. Sample preparation

The equiatomic CoCrFeMnNi HEA was cast in a vacuum induction furnace using high purity metals. The cast ingot was hot-rolled at 900 °C to a thickness reduction of 50%, and then homogenized at 1200 °C for 2 h in Ar atmosphere followed by water-quenching. To refine the grain size, HEA samples were cold-rolled to a thickness reduction of 60%, and subsequently annealed at a furnace temperature of 900 °C for 5 min in Ar atmosphere followed by water-quenching. A commercial 304L SS (stainless steel) sheet with a thickness of 2 mm was used as reference material. The chemical compositions (wt.%) of the two types of materials investigated are listed in Table 1. Samples with dimensions 10 mm × 10 mm × 2 mm were machined from the alloy sheets. Then, they were ground sequentially from 400 to 2500 grit SiC paper, polished with 0.1 μm diamond powder. After that, they were cleaned with deionizer water, alcohol, and then dried in cool air. The electrodes used for the electrochemical tests were connected by a wire welded to the back side of the samples, and sealed with a curing epoxy resin, leaving only one face with a size of 1 cm^2 exposed to the solution. 0.1 M H_2SO_4 solution was used as electrolyte during the testing.

2.2. Microstructural analysis

The starting microstructures of the materials were characterized by back-scatter electron imaging (BSEI) and electron backscatter diffraction (EBSD) using a Zeiss-Merlin and a Zeiss-Crossbeam XB 1540 FIB scanning electron microscope (SEM), respectively. X-ray diffraction (XRD) analysis were conducted using an X-Ray equipment ISO-DEBYEFLEX 3003 equipped with Co Kα (λ = 1.788965 Å) radiation operated at 40 kV and 30 mA.

2.3. Micro-electrochemical corrosion and online in-situ element-resolved analysis

Micro-electrochemical corrosion and online element-resolved measurements were performed in 0.1 M H_2SO_4 (Merck, 96% suprapur) using a scanning flow cell (SFC) with a potentiostat Gamry Reference 600 at ambient pressure and temperature (25 °C). The tip of the microcell was encircled by a silicone O-ring that prevents electrolyte leakage when the cell is pressed onto the sample connected as working electrode. The area that was wetted by the cell was about 1.08 mm^2. The counter electrode (Pt-wire, 0.5 mm, 99.997%, Alfa Aesar) was placed in the inlet channel and the reference electrode (Ag/AgCl, 3 M KCl, reference potential +207 mV vs. standard hydrogen electrode (SHE)) in the outlet channel of the cell. The electrolyte outlet of the SFC was connected to the inductively coupled plasma-mass spectrometer (ICP-MS, NexION 300X, Perkin Elmer) for online in-situ element-resolved analysis. The electrolyte was pumped through the cell at a flow rate of 230 μL min^{-1}. The ICP-MS was calibrated prior to the measurements. The detected intensities of the elements (^{52}Cr, ^{55}Mn, ^{56}Fe, ^{59}Co, ^{60}Ni) were converted to the concentration of dissolved ions. Detailed setup and measurement processes were described in the literature [20]. During the ICP-MS measurement, the concentrations of dissolved ions were detected for three different stages, i.e., open-circuit potential (OCP), holding time and polarization. Between the OCP and polarization stages, a holding time of approximately 5 min was required to ensure a stable testing system. In addition, the cyclic potentiodynamic polarization tests were performed at a scan rate of 0.1 mV s^{-1} with a specimen surface area of 1.0 cm^2. A saturated KCl, Ag/AgCl reference electrode was connected to the cell through a Luggin capillary. All potentials in the present study refer to SHE. The electrochemical impedance spectroscopy (EIS) measurements were conducted in a Solartron system-potentiostat (model 1287A)/frequency response analyzer (model 1260A) workstation with a conventional three-electrode cell. Before the EIS tests, the OCP was measured for 3600 s. The EIS was started with the applied AC amplitude of 10 mV, and the frequency was swept from 100 kHz down to 10 mHz. The impedance data was interpreted by using the Zsimpwin software and equivalent electron circuits. Each experiment was repeated at least three times under the same condition to confirm reproducibility. All EIS measurements were conducted at room temperature (25 °C).

2.4. Compositional analysis of the passive films

To investigate the passive films on the equiatomic HEA and 304L SS, the bulk samples were charged under potentiostatic conditions for 2 h at a potential of +400 mV_{SHE} to produce the stable passive films. The potential was chosen with reference to the characteristic features of the potentiodynamic polarization curve. Then, the specimens were rinsed with distilled water, dried and transferred to the X-ray photoelectron spectroscopy (XPS) analyzer chamber immediately. The compositions of the passive films formed by exposing the specimens to the 0.1 M H_2SO_4 solution were measured by using a Physical Electronics Quantum 2000 ESCA microprobe system in conjunction with monochromatic Al K_α X-ray radiation. The XPS data were analyzed using the commercial software CasaXPS (version 2.3.15), and the peaks were fitted by the mixed Gaussian-Lorentzian functions after Shirley background subtraction. The binding energy (BE) scale was calibrated on a C1 s peak at 285 eV, and all the other peaks obtained by the XPS analysis were calibrated by the standard C1 s peak. XPS analysis for each sample condition was repeated at least three times to confirm reproducibility.

2.5. Immersion tests and surface observation

Immersion tests were carried out in 0.1 M H_2SO_4 solution at room temperature for 30 days. Then, the surface morphology of the tested samples was investigated by using Zeiss-Merlin instrument equipped with energy-dispersive spectrometry (EDS).

3. Results and discussion

3.1. Starting microstructure

Fig. 1 show the inverse pole figure (IPF) maps and back-scattered electron (BSE) morphology of the equiatomic CoCrFeMnNi HEA and 304 L SS, respectively. Both types of materials exhibit recrystallized microstructure with high amounts of annealing twins. The XRD patterns inserted in Fig. 1b_2 confirm the FCC structure with similar lattice parameters in both materials. The average grain sizes of the CoCrFeMnNi HEA and the 304 L SS are ~8 μm and 30 μm, respectively. According to the previous work, grain size, when in the micrometer-range, has no substantial effect on the corrosion of stainless steel [21,22] in sulfuric acid solution. An evident influence occurs only when the average grain size value falls into the nanoscale regime [23,24]

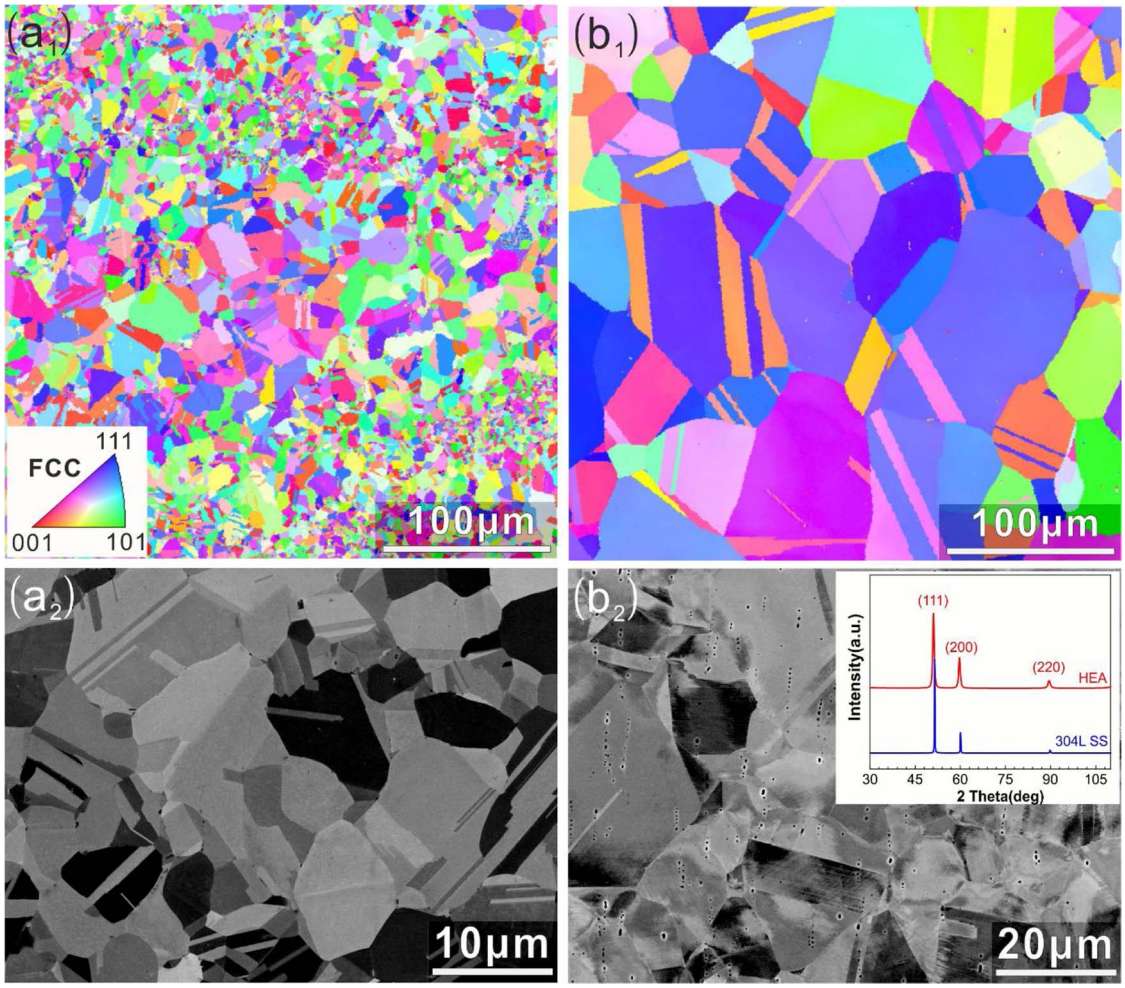

Fig. 1. Starting microstructure of (a_1) (a_2) the equiatomic CoCrFeMnNi HEA and (b_1) (b_2) the 304L SS samples prior to corrosion testing. The inset in (b_2) shows the XRD patterns of the two alloys.

which might be due to the increased diffusion rates along interfaces enabling the elements to migrate faster and form a protective passive film in nano-grained materials [23].

3.2. Electrochemical corrosion behavior and element-resolved online in-situ analysis

Fig. 2 shows the cyclic potentiodynamic polarization curves for the equiatomic HEA and 304L SS in 0.1 M H_2SO_4. No obvious hysteresis loop was observed in the reverse scans, indicating that both HEA and 304L SS are not susceptible to localized corrosion in 0.1 M H_2SO_4 solution at room temperature. In addition, the equiatomic HEA and 304L SS exhibit similar features with a passive potential range extending from the corrosion potential to the onset of transpassivity. Moreover, the passive current density of 304L SS is lower than that of the HEA in 0.1 M H_2SO_4.

Fig. 3 shows the element-resolved online analysis results of the equiatomic HEA and 304L SS in 0.1 M H_2SO_4. The average concentrations of individual dissolved elements corresponding to the open circuit potential (OCP), passive and transpassive regions are also listed. During the OCP time, the equiatomic HEA shows a high dissolution rate of metals and the dissolution of Fe is significant according to the fact that the concentration of Fe ions exceeds that of the other metal ions in 0.1 M H_2SO_4 solution (Fig. 3a). The dissolution of Co, Ni, Mn, and Cr also occur in the equiatomic HEA sample, and the concentration of Co ions (~72.4 μg/L) is slightly higher than that of Ni, Mn, and Cr (~65.6, 60.3, 59.1 μg/L). Interestingly, the concentration of Ni ions is slightly

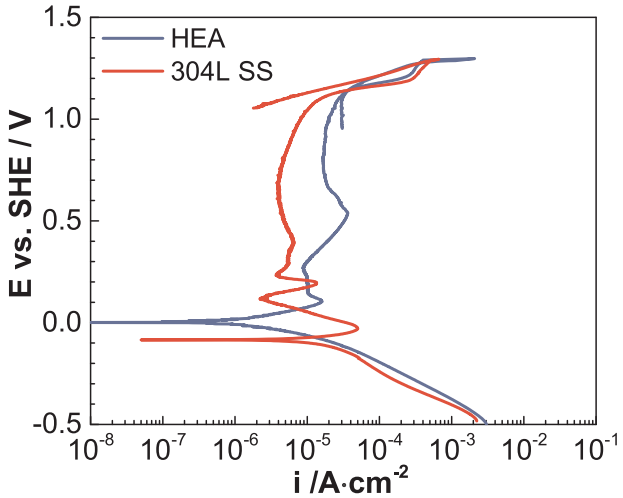

Fig. 2. Cyclic potentiodynamic polarization curves of the equiatomic HEA and 304L SS samples in 0.1 M H_2SO_4 at room temperature.

higher than that of the Mn and Cr ions. These findings suggest that the passive film formed under OCP conditions is not strong enough to prevent the dissolution of metal elements. In the passive region, the dissolution rate decreased significantly due to the formation of a stable passive film, compared to the OCP condition. All the metal elements started dissolution again in the transpassive region and features similar

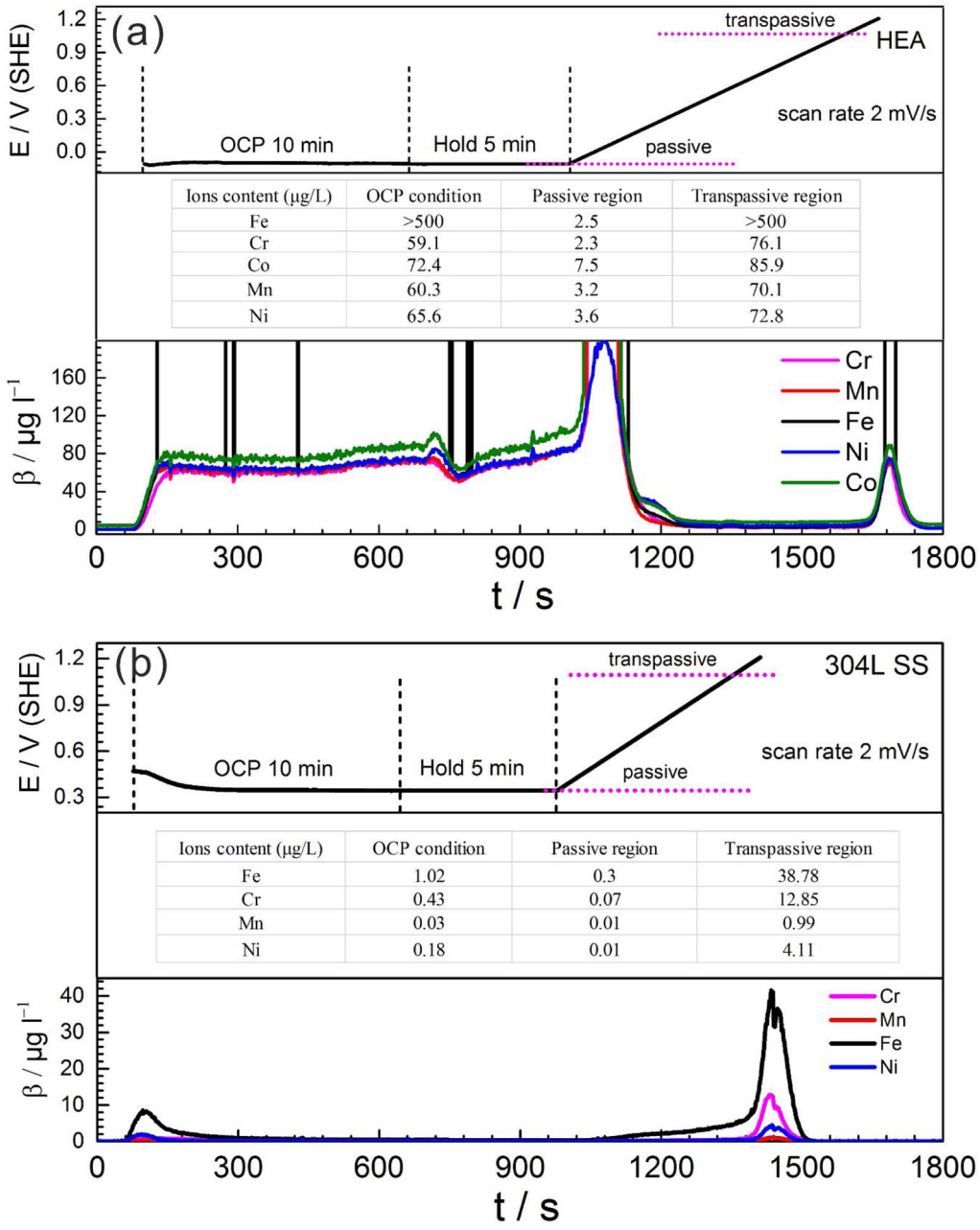

Fig. 3. Electrochemical behaviour and online in-situ element-resolved analysis of the equiatomic CoCrFeMnNi HEA (a) and the 304 L SS (b) in 0.1 M H_2SO_4 (2 mV/s in positive direction). Online ICP-MS dissolution profiles were converted into dissolution concentration values of metal-Cr, Mn, Fe, Ni, Co, shown in pink, red, black, blue and green color codes, respectively. (For interpretation of the references to colour in this figure legend, the reader is referred to the web version of this article.)

to those observed under OCP conditions were found. The specific metal ion concentrations are listed in Fig. 3a. Nevertheless, in the passive regions, a stable passive film of the HEA can be formed to prevent the continuous dissolution of the other elements. No obvious selective dissolution of metal elements was observed.

In terms of the 304 L SS (Fig. 3b), only a very small amount of Fe ions (~1.02 μg/L) and a sub-stoichiometric concentration of Cr dissolve in the solution during the OCP time range. Moreover, only very slight metal ion dissolution was observed during the passive region, as shown in the table inserted into Fig. 3b. In the transpassive region, Fe, Cr, and Ni dissolve in the solution, but their concentrations are relatively low due to the formation of a dense Cr-oxides passive film. The formation of a Cr-oxide passive film on stainless steel is ascribed to the selective dissolution of Fe during passivation, leaving Cr enriched in the passive film [25–27]. However, in the case of the equiatomic CoCrFeMnNi HEA, the dissolution rate of all the elements are of a similar order of magnitude, and no selective dissolution of metal elements is observed during the passivation according to the concentrations of the various metal ions obtained by the online ICP-MS analysis shown above. All these observations suggest that the passive film formed on the 304 L SS is much more stable, and show better anti-corrosion features than the equiatomic CoCrFeMnNi HEA. Literature has shown that the low dissolution rates of elements in stainless steel are due to the presence of a passive film which acts as a barrier for metal dissolution and corrosion [26,28]. Moreover, according to the PDM model [29,30], the passive film contains a high concentration of point defects, such as oxygen vacancies and metal cation vacancies. Compared to the passive film on stainless steel, it can be assumed that the passive film on HEA is highly defective so that the metal ions can easily migrate through the passive film during the dissolution process.

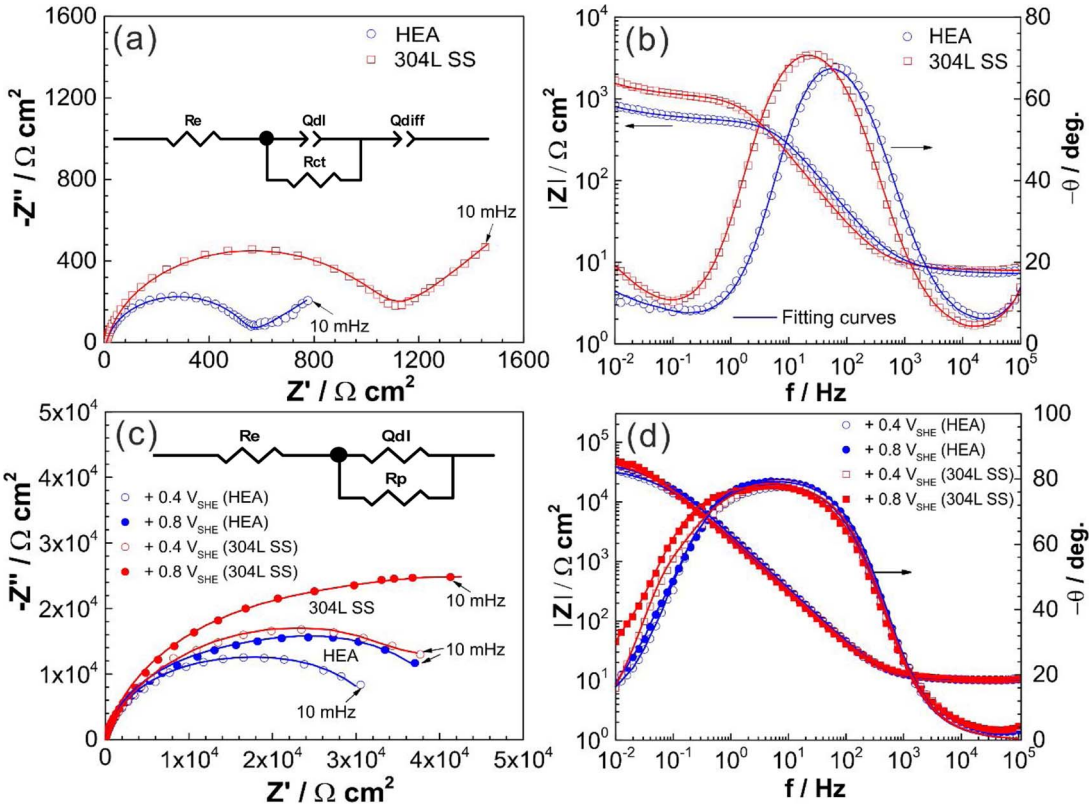

Fig. 4. Nyquist (a) and Bode plots (b) of the equiatomic CoCrFeMnNi HEA and 304L SS in 0.1 M H_2SO_4 under open circuit potential condition. Nyquist (c) and Bode plots (d) of the equiatomic CoCrFeMnNi HEA and 304 L SS in 0.1 M H_2SO_4 after passivation at different potentials. The insert in Fig. 3a and 3c are the electrical equivalent circuits (EECs) for fitting the EIS experimental data. Solid lines refer to the fitting curves.

3.3. Characteristics of the passive films

To understand the corrosion mechanisms of the equiatomic CoCrFeMnNi HEA compared with the 304L SS, we further investigated the characteristics of the passive films formed on the two types of materials by combining electrochemical impedance spectroscopy (EIS) and X-ray photoelectron spectroscopy (XPS). Fig. 4a and b shows the EIS plots of the passive film formed in 0.1 M H_2SO_4 solution under OCP condition. Fig. 4c and 4d show the EIS plots of the passive film formed in 0.1 M H_2SO_4 solution at two potentials. The electrical equivalent circuit (EEC) used for fitting the experimental data has also been inserted in Fig. 4a and c.

In Fig. 4a the Nyquist plots of the two materials display similar features where a depressed capacitive semicircle covers most the high-frequency region and a straight line the low-frequency domain. The appearance of the straight line in the Nyquist plots revealed that the kinetics of the dissolution of surface passive film is limited by diffusion of the oxidation products as previously reported [31]. The diameters of the capacitive semicircle [32] of the equiatomic HEA sample are smaller than those of the 304 L SS, indicating a lower corrosion resistance of the equiatomic HEA compared to the 304 L SS in 0.1 M H_2SO_4 solution. From the Bode plots of the two materials (Fig. 4b), a linear relationship between $\log|Z|$ and $\log f$ is observed in the frequency range of 10^{-3} to 10° Hz. Both slopes are below -1 and the phase angle achieves a maximum value below -90° indicating the pseudocapacitive nature of the passive films [33]. Furthermore, only one time constant was observed in the Bode plots. The value of $|Z|$ at a fixed frequency of 0.1 Hz in the Bode plots usually corresponds to the polarization resistance which reflects the corrosion resistance of the alloy in the solution [34]. As shown in Fig. 4b, the values of $|Z|$ at 0.1 Hz for the equiatomic HEA ($\sim 8.25 \times 10^2\ \Omega\,cm^2$) is lower than that of 304L SS ($\sim 1.7 \times 10^3\ \Omega\,cm^2$), indicating that 304L SS is more corrosion-resistant than the equiatomic HEA in 0.1 M H_2SO_4 solution. This difference in corrosion resistance is attributed to the different composition and thickness of the passive films formed on the samples during immersion in the solution, which was further confirmed by XPS results.

The Nyquist and Bode plots for the two alloys passivated at $+400\ mV_{SHE}$ and $+800\ mV_{SHE}$ are presented in Fig. 4c and d. Significant differences could be observed in the curves obtained at passivation condition compared to that under OCP condition. All the Nyquist plots under passivation conditions are characterized by a somewhat unfinished semi-circle, a feature which is potential dependent. The diameter of the semicircle in the Nyquist plot grows with higher applied potential, indicating an increase in the corrosion resistance. In the Bode plots, at high frequencies the impedance modulus value almost keeps constant and the phase angle is close to zero, indicating a resistive-like behavior [35]. Moreover, at the medium and low frequencies a slanted impedance modulus value and a maximum phase angle are achieved, suggesting a capacitive-like behavior. Compared to the maximum phase angle of the two alloys under OCP conditions (in the range of 68–71°), the maximum phase angle under passivation condition is higher (in the range of 77–81°), indicating a significant improvement in corrosion properties of the two alloys.

In the present study, an EEC model from the literature [31,36] was used to fit the impedance spectra measured under OCP condition. The very small chi-square values ($\sim 10^{-3}$, order of magnitudes) suggest good fitting quality. In the EEC inserted in Fig. 4a, the solution resistance (R_e) is in electrical series with a parallel combination of a constant phase element Q_{dl} and R_{ct}, followed by Q_{diff}. The parameter Q_{dl} represents the surface heterogeneity, indicating the compactness of the passive film. The constant phase element parameter Q (CPE), which has been widely used in EEC analysis, serves in analyzing the frequency dispersion behavior of different corrosion phenomena [37–40]. The

Table 2
Equivalent circuit parameters for impedance spectra of the HEA and 304L SS samples in 0.1 M H_2SO_4 under OCP condition.

Materials	R_e ($\Omega\,cm^2$)	Q_{dl} ($\Omega^{-1}\,cm^{-2}\,s^n$)	n_{dl}	R_{ct} ($\Omega\,cm^2$)	Q_{diff} ($\Omega^{-1}\,cm^{-2}\,s^n$)	n_{diff}	Σc^2
HEA	7.08	6.93×10^{-5}	0.91	512	1.05×10^{-2}	0.45	2.903×10^{-3}
304 L SS	7.81	1.12×10^{-4}	0.92	1028	6.77×10^{-3}	0.55	3.264×10^{-3}

parameter of Q_{diff} was used instead of the Warburg impedance (W) to describe the mass transport process [31]. On the other hand, the EIS was performed in the passive state at two potentials, and the fitting routine was carried out using the EEC from Refs. [41,42] which is inserted in Fig. 4c. The solution resistance (R_e) is in series with a parallel combination of a Q_{dl} unit and R_p (polarization resistance). R_p strongly depends on the passive film, which is also an indication of the good corrosion resistance of the material [43].

Table 2 shows the EEC fitting parameters obtained for the equiatomic HEA and 304 L SS under OCP condition. The value of Q_{dl} obtained for the HEA is lower than that of the 304 L SS, suggesting higher compactness of the passive film on the 304 L SS. The values of n_{dl} are approximately 0.9, suggesting that the value Q_{dl} exhibits intermediate properties between a regular capacitor and a Warburg impedance. In terms of the charge transfer resistance (R_{ct}), the equiatomic HEA sample shows a lower value than the 304L SS. This observation suggests that the passive film formed on the equiatomic HEA has more activated sites, further causing the lower corrosion resistance of the equiatomic HEA. Also, this indicates that the rate of electrochemical reaction occurring at the passive film/electrolyte interface or dissolution rate of the passive film is higher for the equiatomic HEA than that for the 304 L SS in 0.1 M H_2SO_4 solution. Interestingly, the value of Q_{diff} for the equiatomic HEA is one order of magnitude higher than that of the 304 L SS, which suggests that the diffusion coefficient of the metal and oxygen ions is likely one order smaller than that of the equiatomic HEA. The values of Q_{diff} further confirms that the passive film formed on 304L SS is more effective in reducing the rate of diffusion, which contributes to the high corrosion resistance in 0.1 M H_2SO_4 solution [44]. The above findings further indicate that the corrosion process of the equiatomic CoCrFeMnNi HEA and 304L SS are controlled not only by a charge-transfer process but also by a diffusion control process. Table 3 shows the EEC fitting parameters obtained for the equiatomic HEA and 304 L SS at two potentials. The n_{dl} values of the two alloys are lower than 1, indicating that the electrochemical behavior of the passive film is different from the pure capacitive behavior. The R_p values increase with increasing the potential from $+400\,mV_{SHE}$ to $+800\,mV_{SHE}$. Moreover, the R_p values obtained from 304L SS is higher than that of the HEA under the same condition. This suggests that the applied potential (in the passive region) causes the formation of stable and protective passive film for the two alloys. Further, the passive film on 304L SS is more stable with higher protective ability compared to the passive film on the HEA. These findings are consistent to the EIS results obtained under OCP conditions as shown above.

Fig. 5 presents the XPS results of Cr $2p_{3/2}$, Fe $2p_{3/2}$, Ni $2p_{3/2}$, O 1s, Co $2p_{3/2}$ and Mn $2p_{3/2}$ for the passive film formed on the equiatomic CoCrFeMnNi HEA and 304 L SS after passivation 2 h at $+400\,mV_{SHE}$ in 0.1 M H_2SO_4 solution. For both of the two alloys, the Cr $2p_{3/2}$ ionization is split into three constituent peaks (Fig. 5a_1 and b_1), i.e., the metallic state $Cr_{(met)}$ (574.1 eV), Cr_2O_3 (576.3 eV) and Cr $(OH)_3$ (577.1 eV). Based on the intensities of peaks of Cr_2O_3 and $Cr(OH)_3$, the Cr_2O_3 is the primary constituent of the chromium ionisation in the passive film on 304L SS, while the primary constituent of the chromium ionisation in the passive film on the equiatomic HEA is the $Cr(OH)_3$.

Fig. 5a_2 and b_2 show the Fe $2p_{3/2}$ spectra obtained on the passive films. They are separated into several constituent peaks representing the metallic Fe (706.8 eV), Fe_{ox}^{2+} (708.4 eV), Fe_{ox}^{3+} (710 eV) and Fe_{hy}^{3+} (711.8 eV). For both materials, the Fe^{3+} (oxide and hydroxide species) is the primary iron oxidized species as observed from the relative intensity of Fe^{2+} and Fe^{3+} in Fig. 5a_2 and b_2. The deconvolution results of iron species indicate that the iron hydroxide species is the main constituent in the passive film of the equiatomic HEA, and the iron oxide species prevails in the passive film of 304 L SS. A weak single peak component assigned to the metallic nickel was detected in the 304L SS (Fig. 5b_3). The appearance of metallic nickel is probably due to the fact that nickel is less readily oxidized than Fe and Cr [28], and Ni oxide is readily removed during ion sputtering [45]. Previous studies have shown that the amount of nickel present in the passive film of stainless steel is very low, so that it is even had to be distinguished from the background noise [46–48]. However, in the case of the equiatomic HEA, the oxide of Ni in the passive film can be clearly observed. As shown in Fig. 5a_3, the Ni $2p_{3/2}$ spectra are split into four constituent peaks representing the metallic Ni (852.6 eV), Ni_{ox}^{2+} (853.7 eV), Ni_{hy}^{2+} (856.2 eV) and Ni_{sat} (859.2 eV). The relative peak intensities of Ni_{ox}^{2+} and Ni_{hy}^{2+} demonstrate that Ni_{hy}^{2+} is the primary oxidized species in the passive film. Literature shows that the reduction in the presence of Mn oxides in the passive film could improve the stability of the passive film, inducing better resistance to corrosion [49]. This suggests that high content of Mn oxides in the passive film is harmful to the corrosion resistance of the HEA. Pure cobalt has been found to exhibit no transition from active to passive states in diluted sulfuric acid solution [50,51]. Therefore, the existence of cobalt species in the passive film is likely to have no contribution to the corrosion resistance of the HEA. The O1 s spectra obtained from the passive film on the 304L SS are separated into three components (Fig. 5b_4). The O^{2-} species (530.2 eV) are in the form of oxides of Cr and Fe. The peaks at 531.8 eV represent the OH^- species, corresponding to the formation of metal-hydroxide. The third peak at about 533 eV represents bound water (H_2O) in the passive film. However, for the equiatomic HEA (Fig. 5a_4), the peak pertaining to H_2O in the passive film is absent, which is similar to the case of hydrogen charged passive films observed on duplex stainless steel [52]. The bound water can act as an effective species to capture the dissolving metal ions, forming a new film resisting further corrosive attack [53,54]. Moreover, it can be observed that OH^- species are the main constituents of the passive film formed on the equiatomic HEA. The fractions of cationic and metallic species of Cr, Fe, Ni, Mn and Co in the passive film on HEA and 304 L SS were shown in Fig. 5c. The quantitative results reveal that the primary constituents of the passive film on 304 L SS and HEA are chromium oxide and iron

Table 3
Equivalent circuit parameters for impedance spectra of the HEA and 304 L SS samples in 0.1 M H_2SO_4 at two potentials.

Potentials	Materials	R_e ($\Omega\,cm^2$)	Q_{dl} ($\Omega^{-1}\,cm^{-2}\,s^n$)	n_{dl}	R_p ($\Omega\,cm^2$)	$\Sigma\chi^2$
+400 mV	HEA	1.05	8.24×10^{-5}	0.88	3.16×10^4	2.389×10^{-3}
	304 L SS	1.02	7.21×10^{-5}	0.89	3.88×10^4	4.219×10^{-3}
+800 mV	HEA	1.04	8.09×10^{-5}	0.87	4.18×10^4	2.421×10^{-3}
	304L SS	1.05	8.99×10^{-5}	0.86	5.74×10^4	2.187×10^{-3}

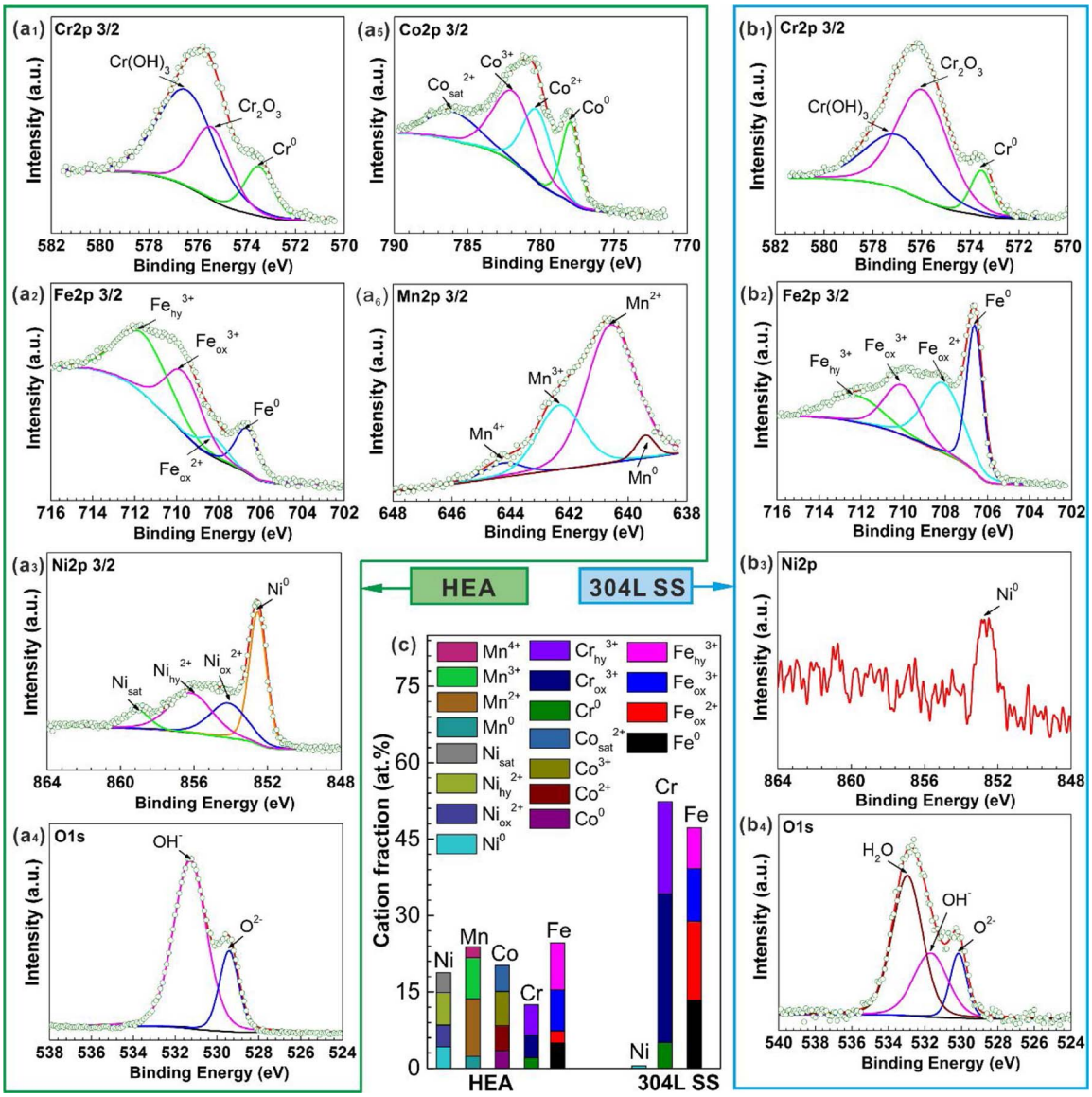

Fig. 5. High resolution XPS spectra of the passive films formed on the equiatomic CoCrFeMnNi HEA (a_1)–(a_6) and the 304L SS (b_1)–(b_4) after passivation for 2 h at +400 mV_{SHE} in 0.1 M H_2SO_4 solution at room temperature. (a_1), (b_1) Cr2p 3/2; (a_2), (b_2) Fe2p 3/2; (a_3), (b_3) Ni2p 3/2; (a_4), (b_4) O 1s; (a_5) Co2p 3/2; (a_6) Mn 2p 3/2. (c) Cationic fractions in the passive film of HEA and 304 L SS obtained by XPS analysis.

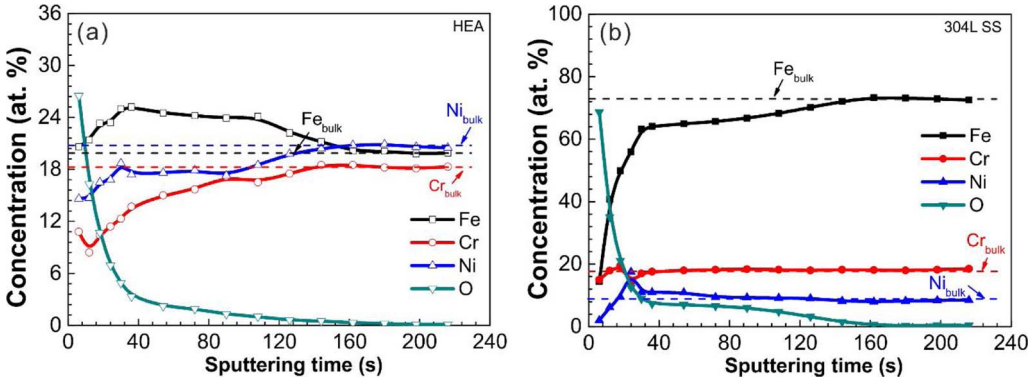

Fig. 6. XPS sputtering depth profiles of the alloy elements in the passive films of the equiatomic CoCrFeMnNi HEA and 304 L SS after passivation 2 h at +400 mV_{SHE} in 0.1 M H_2SO_4 solution at room temperature. (a) HEA and (b) 304L SS.

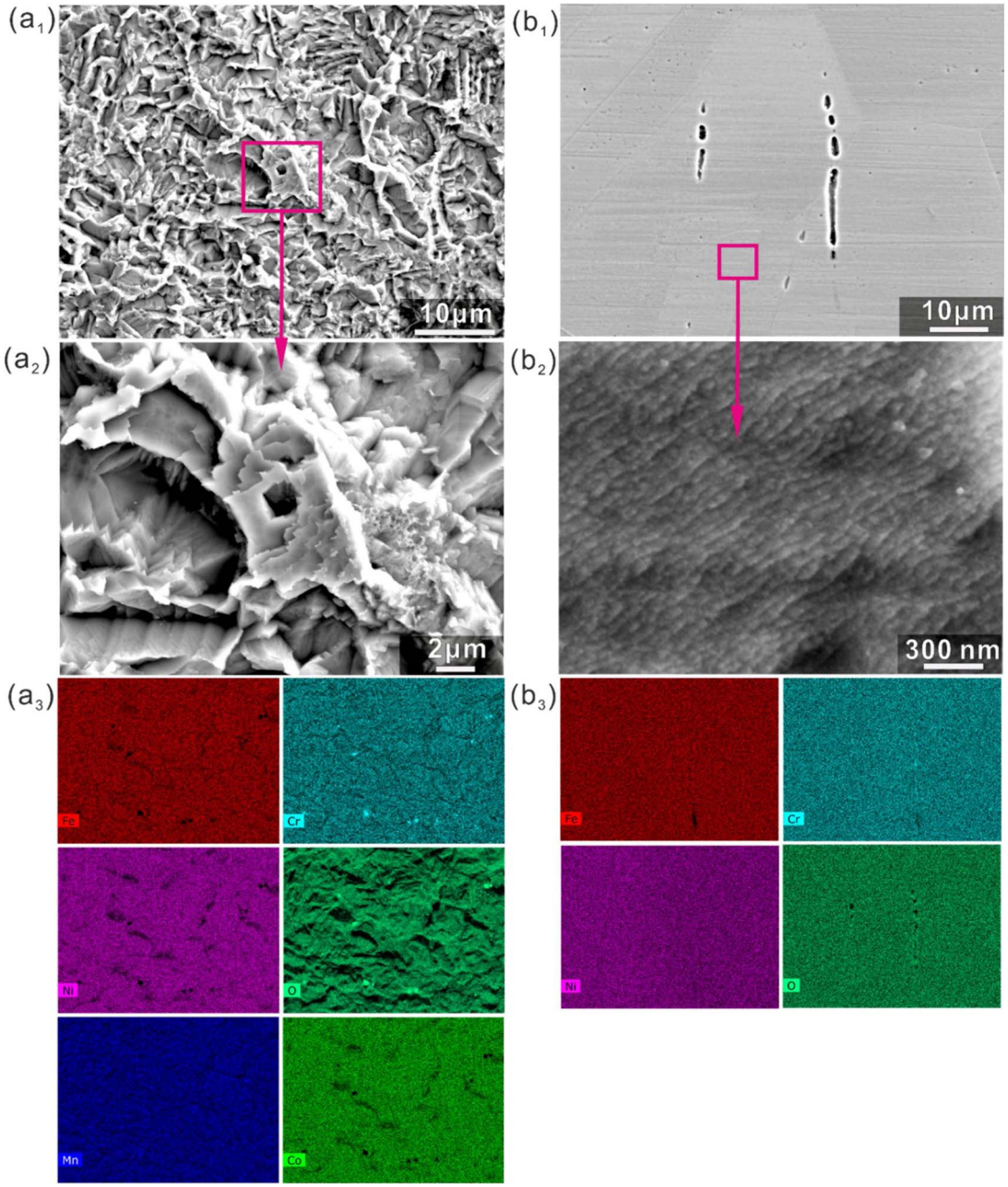

Fig. 7. Surface morphology and EDS mapping of the equiatomic CoCrFeMnNi HEA and 304 L SS after immersion in 0.1 M H_2SO_4 solution for 30 days at room temperature. (a_1), (a_2), (a_3) HEA; (b_1), (b_2), (b_3) 304 L SS.

oxide species, respectively. Also, oxidized species of Cr, Co, Mn, and Ni were detected in the passive film on the HEA (Fig. 5c).

Fig. 6 shows the XPS depth profiles of three main elements in the passive film formed on the two alloys 0.1 M H_2SO_4 solution. The profiles obtained for the equiatomic HEA (Fig. 6a) show that the concentration of oxygen decreases and the concentrations of Fe and Ni increase with the increase in sputtering depth. The concentration of Fe is higher than those of Cr and Ni in the passive film at the initial stage of sputtering. As shown in Fig. 6a, the concentrations of Cr and Ni in the passive film are lower than in the bulk matrix. In the case of 304L SS, a very different depth profile of the elements in the passive film was observed. Fig. 6b shows that the entire passive film is enriched in Cr, and there is a strong enrichment of Ni close to the film/metal interface where Cr is depleted. Additionally, the passive film formed on the 304 L SS is slightly thinner than that on the equiatomic HEA.

3.4. Morphology of corroded surfaces

Fig. 7 shows the surface morphology of the equiatomic HEA and 304L SS after immersion in the 0.1 M H_2SO_4 solution for 30 days at room temperature. The surface of the equiatomic HEA was severely corroded after long time immersion, showing major non-uniform surface exfoliation (Fig. 7a_1 and a_2). The EDS mapping results (Fig. 7a_3) show that there are no corrosion products deposited on the surface. This suggests that the passive film on the equiatomic HEA does not provide effective protection when immerged in 0.1 M H_2SO_4 solution. Fig. 7b_1 shows the surface morphology of 304 L SS after the immersion test. There are some corrosion pits on the surface, which suggests that the sample only suffered from a localized corrosion in 0.1 M H_2SO_4 solution. The corrosion pits were randomly distributed on the sample surface. Moreover, as documented by the inserted high-resolution image in Fig. 7b_2, the surface of the regions without corrosion pits is not smooth

at the nanometer scale. Also, there is no corrosion product deposited on the surface according to the EDS results in Fig. 7b_3. Therefore, we can further verify that the 304L SS is more corrosion-resistant than the HEA in 0.1 M H_2SO_4 solution.

Several previous studies have demonstrated that the corrosion resistance of metallic alloys is highly dependent on the composition and structure of the passive films formed in the solution [28,55,56]. As a result of the present work, the excellent corrosion resistance of 304 L SS can also be ascribed to the formation of a stable passive film exposing to the environment, fully consistent with the literature [53,57]. As shown above, the main composition of the passive film on the 304L SS are Cr and Fe oxides, and the content of Cr in the passive film (> 15 at.%) is even higher than in the bulk matrix. In the case of the equiatomic HEA, the high concentration of Cr could in principle be expected to be also beneficial for the material's corrosion resistance. Likewise, the high Ni content could also be expected to bring down the overall dissolution rates of Fe and Cr. The corrosion resistance of the equiatomic HEA is lower than that of the 304L SS since its passive film formed in 0.1 M H_2SO_4 is very unstable. At least three mechanisms are responsible for the unstable passive film on the equiatomic HEA. First, the Cr content in the passive film is much lower than that in the 304 L SS passive film. This is due to that no obvious selective dissolution of Mn, Co, Ni and Fe occur during the surface passivation on the equiatomic HEA in 0.1 M H_2SO_4 solution (Fig. 3a). Also a Cr-depleted zone in the passive film has been observed on the HEA. Second, mixed Fe-, Cr- and Ni-hydroxides are the main components of the passive film formed on the equiatomic HEA. Compared with oxides of Cr and Fe, the Cr, Fe, and Ni hydroxides show detrimental effects on the corrosion resistance in 0.1 M H_2SO_4 solution. Third, the lack of bound water in the passive film on the equiatomic HEA also shows negative effects on the corrosion resistance.

4. Conclusions

The corrosion behavior and composition of the passive films of an equiatomic CoCrFeMnNi high-entropy alloy (HEA) and a 304 L SS in 0.1 M H_2SO_4 solution were investigated in detail by using an in-situ online element-resolved corrosion analysis method and X-ray photoelectron spectroscopy. The main conclusions are:

1. Both the equiatomic HEA and the 304L SS show good capability of forming passive films, but no obvious selective dissolution of metal elements occurred during the passivation on the surface of the equiatomic HEA.
2. The basic corrosion mechanisms of the equiatomic HEA and 304L SS are similar when exposed to dilute sulfuric acid solution under OCP condition, showing a mixed charge transfer and diffusion control process.
3. The main constituents of the passive film on the equiatomic HEA are hydroxides of Cr, Fe and Ni mixed with Mn, Co oxides, while the passive film on 304L SS shows as main components oxides of Cr and Fe. Also, the Cr content in the passive film on the equiatomic HEA is much below that found in the 304L SS passive film.
4. There is a Cr-depleted and Fe-enriched zone in the passive film on the equiatomic HEA. The thickness of the passive film on the equiatomic HEA is thicker than that on the 304L SS.

Acknowledgment

The authors gratefully acknowledge the support from the Alexander von Humboldt Stiftung of Germany.

References

[1] J.W. Yeh, S.K. Chen, S.J. Lin, J.Y. Gan, T.S. Chin, T.T. Shun, C.H. Tsau, S.Y. Chang, Adv. Eng. Mater. 6 (2004) 299–303.
[2] B. Cantor, I. Chang, P. Knight, A. Vincent, Mater. Scie. Eng.: A 375 (2004) 213–218.
[3] Y. Zhang, T.T. Zuo, Z. Tang, M.C. Gao, K.A. Dahmen, P.K. Liaw, Z.P. Lu, Prog. Mater. Sci. 61 (2014) 1–93.
[4] B. Gludovatz, A. Hohenwarter, D. Catoor, E.H. Chang, E.P. George, R.O. Ritchie, Science 345 (2014) 1153–1158.
[5] Z. Li, K. Pradeep, Y. Deng, D. Raabe, C. Tasan, Nature 534 (2016) 227–227.
[6] F. Otto, A. Dlouhý, C. Somsen, H. Bei, G. Eggeler, E.P. George, Acta Mater. 61 (2013) 5743–5755.
[7] Z. Han, N. Chen, S. Zhao, L. Fan, G. Yang, Y. Shao, K. Yao, Intermetallics 84 (2017) 153–157.
[8] C.P. Lee, C.C. Chang, Y.Y. Chen, J.W. Yeh, H.C. Shih, Corros. Sci. 50 (2008) 2053–2060.
[9] Y.L. Chou, Y.C. Wang, J.W. Yeh, H.C. Shih, Corros. Sci. 52 (2010) 3481–3491.
[10] Y. Shi, B. Yang, X. Xie, J. Brechtl, K.A. Dahmen, P.K. Liaw, Corros. Sci. 119 (2017) 33–45.
[11] R.B. Nair, H.S. Arora, S. Mukherjee, S. Singh, H. Singh, H.S. Grewal, Ultrason. Sonochem. 41 (2018) 252–260.
[12] A. Rodriguez, J.H. Tylczak, M. Ziomek-Moroz, ECS Trans. 77 (2017) 741–752.
[13] Q. Ye, K. Feng, Z. Li, F. Lu, R. Li, J. Huang, Y. Wu, Appl. Surf. Sci. 396 (2017) 1420–1426.
[14] H.H. Uhlig, Corros. Sci. 19 (1979) 777–791.
[15] G. Burstein, P. Pistorius, S. Mattin, Corros. Sci. 35 (1993) 57–62.
[16] P. Pistorius, G. Burstein, Corros. Sci. 36 (1994) 525–538.
[17] G. Burstein, G. Ilevbare, Corros. Sci. 38 (1996) 2257–2265.
[18] S. Ziemniak, M. Hanson, Corros. Sci. 44 (2002) 2209–2230.
[19] S. Ma, S. Zhang, J. Qiao, Z. Wang, M. Gao, Z. Jiao, H. Yang, Y. Zhang, Intermetallics 54 (2014) 104–109.
[20] S.O. Klemm, A. Karschin, A.K. Schuppert, A.A. Topalov, A.M. Mingers, I. Katsounaros, K.J.J. Mayrhofer, J. Electroanal. Chem. 677–680 (2012) 50–55.
[21] A. Di Schino, J. Kenny, J. Mater. Sci. Lett. 21 (2002) 1631–1634.
[22] K. Ralston, N. Birbilis, Corrosion 66 (2010) (075005-075005-075013).
[23] K.S. Raja, S.A. Namjoshi, M. Misra, Mater. Lett. 59 (2005) 570–574.
[24] X. Wang, D. Li, Electrochim. Acta 47 (2002) 3939–3947.
[25] J. Castle, J. Qiu, Corros. Sci. 29 (1989) 591–603.
[26] D. Hamm, K. Ogle, C.-O. Olsson, S. Weber, D. Landolt, Corros. Sci. 44 (2002) 1443–1456.
[27] S. Haupt, H.-H. Strehblow, J. Electroanal. Chem. Interfacial Electrochem. 216 (1987) 229–240.
[28] C.-O. Olsson, D. Landolt, Electrochim. Acta 48 (2003) 1093–1104.
[29] D.D. Macdonald, J. Electrochem. Soc. 139 (1992) 3434–3449.
[30] C. Chao, L. Lin, D. Macdonald, J. Electrochem. Soc. 128 (1981) 1187–1194.
[31] A.A. Hermas, M.S. Morad, Corros. Sci. 50 (2008) 2710–2717.
[32] C. Della Rovere, J. Alano, R. Silva, P. Nascente, J. Otubo, S. Kuri, Corros. Sci. 57 (2012) 154–161.
[33] M. Ray, V. Singh, J. Electrochem. Soc. 158 (2011) C359–C368.
[34] C.A. Della Rovere, J.H. Alano, R. Silva, P.A.P. Nascente, J. Otubo, S.E. Kuri, Corros. Sci. 57 (2012) 154–161.
[35] S. Fajardo, D. Bastidas, M. Criado, J. Bastidas, Electrochim. Acta 129 (2014) 160–170.
[36] A. Kocijan, D.K. Merl, M. Jenko, Corros. Sci. 53 (2011) 776–783.
[37] H. Ashassi-Sorkhabi, D. Seifzadeh, M. Hosseini, Corros. Sci. 50 (2008) 3363–3370.
[38] Y. Qiang, S. Zhang, L. Guo, X. Zheng, B. Xiang, S. Chen, Corros. Sci. 119 (2017) 68–78.
[39] Z. Cui, L. Wang, H. Ni, W. Hao, C. Man, S. Chen, X. Wang, Z. Liu, X. Li, Corros. Sci. 118 (2017) 31–48.
[40] Y. Wang, Y. Qiu, Z. Chen, X. Guo, Corros. Sci. 118 (2017) 96–108.
[41] M. BenSalah, R. Sabot, E. Triki, L. Dhouibi, P. Refait, M. Jeannin, Corros. Sci. 86 (2014) 61–70.
[42] D. Wallinder, J. Pan, C. Leygraf, A. Delblanc-Bauer, Corros. Sci. 41 (1998) 275–289.
[43] S. Marcelin, N. Pébère, S. Régnier, Electrochim. Acta 87 (2013) 32–40.
[44] C. Liu, Q. Bi, A. Leyland, A. Matthews, Corros. Sci. 45 (2003) 1257–1273.
[45] M. Montemor, A. Simões, M. Ferreira, M.D.C. Belo, Corros. Sci. 41 (1999) 17–34.
[46] C. Clayton, Y. Lu, J. Electrochem. Soc. 133 (1986) 2465–2473.
[47] A. Kocijan, Č. Donik, M. Jenko, Corros. Sci. 49 (2007) 2083–2098.
[48] C. Abreu, M. Cristóbal, R. Losada, X. Nóvoa, G. Pena, M. Pérez, Electrochim. Acta 49 (2004) 3049–3056.
[49] Y. Zhang, X. Zhu, Corros. Sci. 41 (1999) 1817–1833.
[50] W. Tomlinson, C. Linzell, J. Mater. Sci. 23 (1988) 914–918.
[51] A.M. Human, B. Roebuck, H.E. Exner, Mater. Sci. Eng.: A 241 (1998) 202–210.
[52] H. Luo, Z. Li, Y.-H. Chen, D. Ponge, M. Rohwerder, D. Raabe, Electrochem. Commun. 79 (2017) 28–32.
[53] G. Okamoto, Corros. Sci. 13 (1973) 471–489.
[54] G. Okamoto, T. Shibata, Nature 206 (1965) 1350.
[55] G. Burstein, P. Marshall, Corros. Sci. 23 (1983) 125–137.
[56] G. Ilevbare, G. Burstein, Corros. Sci. 43 (2001) 485–513.
[57] M. Abdallah, Mater. Chem. Phys. 82 (2003) 786–792.